

















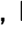





















































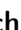

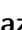
















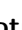






































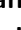



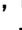

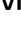












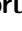

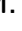





















































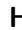



Search for CP violation in $D_{(s)}^+ \rightarrow K_S^0 K^- \pi^+ \pi^+$ decays using triple and quadruple products

The Belle and Belle II Collaborations

L. Aggarwal , H. Ahmed , H. Aihara , N. Akopov , A. Aloisio , N. Alhubiti , N. Anh Ky , D. M. Asner , H. Atmacan , V. Aushev , M. Aversano , R. Ayad , V. Babu , H. Bae , N. K. Baghel , S. Bahinipati , P. Bambade , Sw. Banerjee , J. Baudot , A. Baur , A. Beaubien , F. Becherer , J. Becker , J. V. Bennett , F. U. Bernlochner , V. Bertacchi , M. Bertemes , E. Bertholet , M. Bessner , S. Bettarini , V. Bhardwaj , F. Bianchi , T. Bilka , D. Biswas , A. Bobrov , D. Bodrov , A. Boschetti , A. Bozek , M. Bračko , P. Branchini , R. A. Briere , T. E. Browder , A. Budano , S. Bussino , M. Campajola , L. Cao , G. Casarosa , C. Cecchi , J. Cerasoli , M.-C. Chang , P. Chang , P. Cheema , B. G. Cheon , K. Chilikin , K. Chirapatpimol , H.-E. Cho , K. Cho , S.-J. Cho , S.-K. Choi , S. Choudhury , J. Cochran , L. Corona , J. X. Cui , E. De La Cruz-Burelo , S. A. De La Motte , G. De Nardo , G. De Pietro , R. de Sangro , M. Destefanis , R. Dhamija , A. Di Canto , F. Di Capua , J. Dingfelder , Z. Doležal , T. V. Dong , M. Dorigo , S. Dubey , K. Dugic , G. Dujany , P. Ecker , D. Epifanov , J. Eppelt , P. Feichtinger , T. Ferber , T. Fillinger , C. Finck , G. Finocchiaro , A. Fodor , F. Forti , B. G. Fulsom , A. Gabrielli , E. Ganiev , M. Garcia-Hernandez , R. Garg , G. Gaudino , V. Gaur , A. Gaz , A. Gellrich , G. Ghevondyan , D. Ghosh , H. Ghumaryan , G. Giakoustidis , R. Giordano , A. Giri , P. Gironella Gironell , B. Gobbo , R. Godang , O. Gogota , P. Goldenzweig , W. Gradl , E. Graziani , Z. Gruberová , Y. Guan , K. Gudkova , I. Haide , Y. Han , T. Hara , H. Hayashii , S. Hazra , C. Hearty , A. Heidelberg , I. Heredia de la Cruz , T. Higuchi , M. Hoek , M. Hohmann , R. Hoppe , P. Horak , C.-L. Hsu , T. Humair , T. Iijima , N. Ipsita , A. Ishikawa , R. Itoh , M. Iwasaki , P. Jackson , W. W. Jacobs , E.-J. Jang , Q. P. Ji , S. Jia , Y. Jin , A. Johnson , K. K. Joo , H. Junkerkalefeld , J. Kandra , K. H. Kang , S. Kang , G. Karyan , T. Kawasaki , F. Keil , C. Ketter , C. Kiesling , C.-H. Kim , D. Y. Kim , J.-Y. Kim , K.-H. Kim , Y.-K. Kim , K. Kinoshita , P. Kodyš , T. Koga , S. Kohani , K. Kojima , A. Korobov , S. Korpar , E. Kovalenko , R. Kowalewski , P. Krizan , P. Krokovny , T. Kuhr , Y. Kulii , R. Kumar , K. Kumara , T. Kunigo , A. Kuzmin , Y.-J. Kwon , Y.-T. Lai , K. Lalwani , T. Lam , T. S. Lau , M. Laurenza , R. Leboucher , F. R. Le Diberder , M. J. Lee , C. Lemettais , P. Leo , C. Li , L. K. Li

Q. M. Li , W. Z. Li , Y. Li , Y. B. Li , Y. P. Liao , J. Libby , J. Lin ,
 M. H. Liu , Q. Y. Liu , Y. Liu , Z. Q. Liu , D. Liventsev , S. Longo ,
 T. Lueck , C. Lyu , M. Maggiora , S. P. Maharana , R. Maiti , G. Mancinelli ,
 R. Manfredi , E. Manoni , M. Mantovano , D. Marcantonio , S. Marcello ,
 C. Marinas , C. Martellini , A. Martens , A. Martini , T. Martinov ,
 L. Massaccesi , S. K. Maurya , J. A. McKenna , R. Mehta , F. Meier ,
 M. Merola , C. Miller , M. Mirra , S. Mitra , S. Mondal , S. Moneta ,
 H.-G. Moser , I. Nakamura , M. Nakao , M. Naruki , Z. Natkaniec ,
 A. Natochii , M. Nayak , G. Nazaryan , M. Neu , S. Nishida , S. Ogawa ,
 H. Ono , F. Otani , E. R. Oxford , G. Pakhlova , E. Paoloni , S. Pardi ,
 H. Park , J. Park , K. Park , S.-H. Park , A. Passeri , T. K. Pedlar ,
 I. Peruzzi , R. Pestotnik , M. Piccolo , L. E. Piilonen , T. Podobnik ,
 S. Pokharel , C. Praz , S. Prell , E. Prencipe , M. T. Prim , I. Prudiiev ,
 H. Purwar , P. Rados , G. Raeuber , S. Raiz , N. Rauls , M. Reif , S. Reiter ,
 M. Remnev , L. Reuter , I. Ripp-Baudot , G. Rizzo , M. Roehrken ,
 J. M. Roney , A. Rostomyan , N. Rout , Y. Sakai , D. A. Sanders ,
 S. Sandilya , L. Santelj , V. Savinov , B. Scavino , S. Schneider , M. Schnepf ,
 C. Schwanda , A. J. Schwartz , Y. Seino , A. Selce , K. Senyo , J. Serrano ,
 M. E. Sevier , C. Sfienti , W. Shan , C. Sharma , X. D. Shi , T. Shillington ,
 T. Shimasaki , J.-G. Shiu , D. Shtol , B. Shwartz , A. Sibidanov , F. Simon ,
 J. B. Singh , J. Skorupa , R. J. Sobie , M. Sobotzik , A. Soffer , A. Sokolov ,
 E. Solovieva , S. Spataro , B. Spruck , W. Song , M. Starič , P. Stavroulakis ,
 S. Stefkova , R. Stroili , J. Strube , Y. Sue , M. Sumihama , K. Sumisawa ,
 W. Sutcliffe , N. Suwonjandee , H. Svidras , M. Takizawa , U. Tamponi ,
 K. Tanida , F. Tenchini , A. Thaller , O. Tittel , R. Tiwary , E. Torassa ,
 K. Trabelsi , I. Tsaklidis , I. Ueda , K. Unger , Y. Unno , K. Uno , S. Uno ,
 P. Urquijo , S. E. Vahsen , R. van Tonder , M. Veronesi , V. S. Vismaya ,
 L. Vitale , V. Vobbiliseti , R. Volpe , M. Wakai , S. Wallner , M.-Z. Wang ,
 X. L. Wang , Z. Wang , A. Warburton , S. Watanuki , C. Wessel , X. P. Xu ,
 B. D. Yabsley , S. Yamada , W. Yan , J. Yelton , J. H. Yin , C. Z. Yuan ,
 L. Zani , F. Zeng , J. S. Zhou , Q. D. Zhou , V. I. Zhukova , R. Žlebčik 

ABSTRACT: We perform the first search for CP violation in $D_{(s)}^+ \rightarrow K_S^0 K^- \pi^+ \pi^+$ decays. We use a combined data set from the Belle and Belle II experiments, which study e^+e^- collisions at center-of-mass energies at or near the $\Upsilon(4S)$ resonance. We use 980 fb^{-1} of data from Belle and 428 fb^{-1} of data from Belle II. We measure six CP -violating asymmetries that are based on triple products and quadruple products of the momenta of final-state particles, and also the particles' helicity angles. We obtain a precision at the level of 0.5% for $D^+ \rightarrow K_S^0 K^- \pi^+ \pi^+$ decays, and better than 0.3% for $D_s^+ \rightarrow K_S^0 K^- \pi^+ \pi^+$ decays. No evidence of CP violation is found. Our results for the triple-product asymmetries are the most precise to date for singly-Cabibbo-suppressed D^+ decays. Our results for the other asymmetries are the first such measurements performed for charm decays.

ARXIV EPRINT: [1234.56789](https://arxiv.org/abs/1234.56789)

Contents

1	Introduction	1
2	Methodology	2
3	Detector and data set	4
4	Event selection	5
5	\mathcal{A}_{CP}^X measurement	6
6	Systematic uncertainties	9
7	Combined result and summary	11
A	Simultaneously fitted distributions for $D_{(s)}^+$ data	11
B	Triple- and quadruple-product distributions	11

1 Introduction

The violation of charge-conjugation plus parity (CP) symmetry holds significant importance in particle physics, as it is essential for explaining the matter-antimatter imbalance in the Universe [1]. Within the Standard Model (SM), CP violation (CPV) arises from a complex phase in the Cabibbo-Kobayashi-Maskawa (CKM) matrix [2]. However, this source is insufficient to explain the observed matter-antimatter imbalance, and thus we conclude there must be other sources of CPV , presumably arising from new physics (NP) beyond the SM.

In the SM, CPV in the charm sector arises at the level of $\mathcal{O}(10^{-3})$ or less [3–5], and observing CPV significantly above this level would be interpreted as a sign of NP [6–9]. Various methods have been used to search for CPV in charm decays [10]: measuring differences in decay widths, searching for differences in decay-time distributions or regions of phase-space, measuring triple-product asymmetries, measuring decay asymmetry parameters in baryonic decays, and performing amplitude analyses and an “energy test” [11] of multi-body decays. To date, the only observation of CPV in charm was reported by the LHCb experiment [12], which measured a difference between the asymmetries A_{CP}^{KK} and $A_{CP}^{\pi\pi}$ for $D^0 \rightarrow K^+K^-$ and $D^0 \rightarrow \pi^+\pi^-$ decays. The asymmetry A_{CP} is the difference between partial widths of a D and a \bar{D} divided by their sum; a nonzero value mainly arises from *direct CPV*, i.e., interference between two or more decay amplitudes to the same final state. The effect is proportional to $\sin \delta \sin \phi$, where δ is the strong phase difference between the two amplitudes, and ϕ is the weak phase difference.

Four-body decays of charmed mesons typically proceed via intermediate resonances, and the corresponding amplitudes interfere with one another. Thus, these decays offer a promising opportunity to observe CPV . One observable sensitive to CPV in $D \rightarrow h_1 h_2 h_3 h_4$ ($h = \pi, K, \eta$, etc.) decays is the “triple product” $C_{\text{TP}} \equiv (\vec{p}_1 \times \vec{p}_2) \cdot \vec{p}_3$, where the momenta of the final state particles $\vec{p}_{1,2,3}$ are measured in the rest frame of the D . A difference between the C_{TP} distribution for a D decay and the corresponding \bar{C}_{TP} distribution for a \bar{D} decay is CP -violating. To quantify the difference, the asymmetry about zero for the C_{TP} distribution is compared to the asymmetry about zero for the \bar{C}_{TP} distribution; the difference is denoted $\mathcal{A}_{CP}^{\text{TP}}$. Unlike the asymmetry in partial widths A_{CP} , the triple-product asymmetry $\mathcal{A}_{CP}^{\text{TP}}$ is proportional to $\cos \delta \sin \phi$ [13–15], i.e., it reaches its maximum value at $\delta = 0$. Several experiments have searched for CPV using triple-product asymmetries in four-body D decays [10], thus far without success. Here we measure the triple-product asymmetry for the four-body decays¹ $D^+ \rightarrow K_S^0 K^- \pi^+ \pi^+$ and $D_s^+ \rightarrow K_S^0 K^- \pi^+ \pi^+$. The first mode is singly Cabibbo-suppressed, like the $D^0 \rightarrow K^+ K^-$ and $D^0 \rightarrow \pi^+ \pi^-$ decays for which CPV was observed. The dominant intermediate process, $D^+ \rightarrow \bar{K}^{*0} K^{*+}$, involves tree, annihilation, and “penguin” amplitudes as shown in figure 1. These amplitudes interfere with one another, potentially giving rise to CPV . In addition to measuring the triple-product asymmetry, we also measure the asymmetry for the “quadruple product” $C_{\text{QP}} \equiv (\vec{p}_1 \times \vec{p}_2) \cdot (\vec{p}_3 \times \vec{p}_4)$. This observable is P -even and T -even, unlike the triple product, which is P -odd and T -odd. Quadruple-product asymmetries are discussed as a method for measuring CPV in refs. [15–17]. Finally, we measure asymmetries in helicity angle distributions, which can also exhibit CP violation [16, 18]. To date, quadruple-product asymmetries and asymmetries in helicity angle distributions have not yet been studied for multibody charm decays.

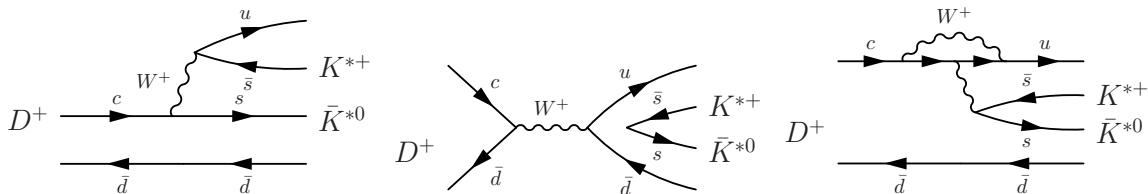


Figure 1. Tree (left), annihilation (center), and “penguin” (right) diagrams contributing to $D^+ \rightarrow \bar{K}^{*0} K^{*+}$. This decay is expected to be the dominant process for the four-body decay $D^+ \rightarrow K_S^0 K^- \pi^+ \pi^+$.

2 Methodology

The topology of $D_{(s)}^+ \rightarrow K_S^0 K^- \pi^+ \pi^+$ decays is shown in figure 2. The angle in the $D_{(s)}^+$ rest frame between the decay planes of the $K_S^0 \pi^+$ pair and the $K^- \pi^+$ pair is denoted ϕ . Also shown are two helicity angles, $\theta_{K_S^0}$ and θ_{K^-} . These are defined as the angle in the

¹For the event selections and analysis procedure, charge-conjugate modes are implicitly included unless noted otherwise.

$K_S^0 \pi^+$ or $K^- \pi^+$ rest frame between the kaon momentum and the direction opposite that of the $D_{(s)}^+$ momentum.

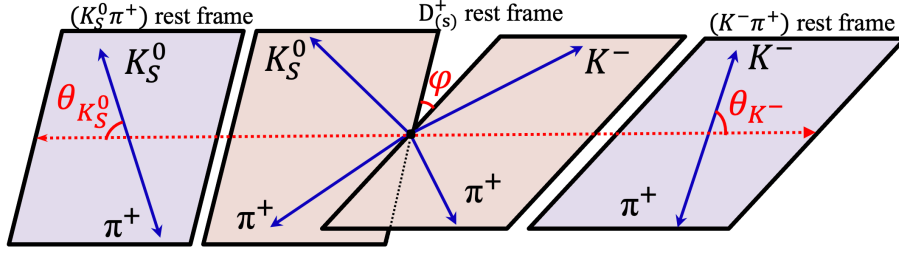


Figure 2. Decay topology for $D_{(s)}^+ \rightarrow K_S^0 K^- \pi^+ \pi^+$. The innermost decay planes, as drawn, correspond to the $D_{(s)}^+$ rest frame; the outermost decay planes, as drawn, correspond to the $K_S^0 \pi^+$ and $K^- \pi^+$ rest frames. The red dashed line denotes the direction of the $(K\pi)$ system's momentum in the $D_{(s)}^+$ rest frame, and the direction opposite the $D_{(s)}^+$ momentum in the $(K\pi)$ system's rest frame.

The triple and quadruple products are defined as:

$$C_{\text{TP}} = (\vec{p}_{K^-} \times \vec{p}_{\pi_h^+}) \cdot \vec{p}_{K_S^0}, \quad (2.1)$$

$$C_{\text{QP}} = (\vec{p}_{K^-} \times \vec{p}_{\pi_l^+}) \cdot (\vec{p}_{K_S^0} \times \vec{p}_{\pi_l^+}), \quad (2.2)$$

where the subscripts “ h ” or “ l ” denote the pion with the higher or lower momentum, respectively. All momenta are measured in the $D_{(s)}^+$ rest frame.² In addition to searching for CPV using C_{TP} and C_{QP} , we also use the product $C_{\text{TP}}C_{\text{QP}}$ and three functions of the helicity angles: $\cos \theta_{K_S^0} \cos \theta_{K^-}$, $C_{\text{TP}} \cos \theta_{K_S^0} \cos \theta_{K^-}$, and $C_{\text{QP}} \cos \theta_{K_S^0} \cos \theta_{K^-}$. The signs of the observables C_{QP} , C_{TP} , and $C_{\text{TP}}C_{\text{QP}}$ are the same as those of $\cos \varphi$, $\sin \varphi$, and $\sin(2\varphi)$, respectively. The sign of $C_{\text{TP}} \cos \theta_{K_S^0} \cos \theta_{K^-}$ is the same as that of a term in the angular distribution of $D \rightarrow V_a V_b$, $V \rightarrow P_1 P_2$ decays[16]: $d_{1,0}^2(\theta_a) d_{1,0}^2(\theta_b) \sin \varphi$, which is proportional to $\sin(2\theta_a) \sin(2\theta_b) \sin \varphi$. The term $C_{\text{QP}} \cos \theta_{K_S^0} \cos \theta_{K^-}$ has the same sign as another term, $d_{1,0}^2(\theta_a) d_{1,0}^2(\theta_b) \cos \varphi$, which is proportional to $\sin(2\theta_a) \sin(2\theta_b) \cos \varphi$. In these expressions, V and P denote vector and pseudoscalar mesons, and the d 's denote Wigner d functions [19, 20]. We thus measure six observables, $X = C_{\text{TP}}$, C_{QP} , $C_{\text{TP}}C_{\text{QP}}$, $\cos \theta_{K_S^0} \cos \theta_{K^-}$, $C_{\text{TP}} \cos \theta_{K_S^0} \cos \theta_{K^-}$, and $C_{\text{QP}} \cos \theta_{K_S^0} \cos \theta_{K^-}$, the signs of which correspond to the signs of different combinations of $\sin \varphi$, $\cos \varphi$, $\cos \theta_{K_S^0}$, and $\cos \theta_{K^-}$.

For each observable, we measure the asymmetry about zero for both $D_{(s)}^+$ and $D_{(s)}^-$ decays:

$$A_X(D_{(s)}^+) \equiv \frac{N(D_{(s)}^+, X > 0) - N(D_{(s)}^+, X < 0)}{N(D_{(s)}^+, X > 0) + N(D_{(s)}^+, X < 0)} \quad (2.3)$$

$$A_{\bar{X}}(D_{(s)}^-) \equiv \frac{N(D_{(s)}^-, \bar{X} > 0) - N(D_{(s)}^-, \bar{X} < 0)}{N(D_{(s)}^-, \bar{X} > 0) + N(D_{(s)}^-, \bar{X} < 0)}, \quad (2.4)$$

²For C_{TP} , the choice of three out of four final state momenta does not impact the measurement, as the total momentum sums to zero. For C_{QP} , the combinations are chosen to be similar to C_{TP} .

where N denotes the yield of $D_{(s)}^+$ or $D_{(s)}^-$ decays. For the observables proportional to C_{TP} , which is the product of a polar vector and an axial vector, \bar{X} is multiplied by -1 to account for the oddness of C_{TP} under a parity transformation. With this extra factor, A_X and $A_{\bar{X}}$ are CP -conjugate quantities for all the observables, and any difference violates CP . We quantify the difference with

$$\mathcal{A}_{CP}^X \equiv \frac{A_X(D_{(s)}^+) - A_{\bar{X}}(D_{(s)}^-)}{2}, \quad (2.5)$$

where $\mathcal{A}_{CP}^X \neq 0$ indicates CP violation.

3 Detector and data set

The Belle detector [21] was a large-solid-angle spectrometer that operated at the KEKB asymmetric-energy e^+e^- collider [22, 23]. It had a cylindrical geometry and consisted of a silicon vertex detector (SVD), a central drift chamber (CDC), an array of aerogel threshold Cherenkov counters (ACC), a barrel-like arrangement of time-of-flight scintillation counters (TOF), and an electromagnetic calorimeter (ECL) based on CsI(Tl) crystals. These components were located inside a superconducting solenoid coil that provided a 1.5 T magnetic field. The iron flux-return of the magnet was instrumented with resistive-plate chambers (KLM) to detect muons and K_L^0 mesons. More details on the Belle detector are provided in refs. [21, 24].

The Belle II detector [25], operates at the SuperKEKB asymmetric-energy e^+e^- collider [26] and also has a cylindrical geometry. It includes a two-layer silicon-pixel detector (PXD) [27, 28] surrounded by a four-layer double-sided silicon-strip detector [29] and a 56-layer central drift chamber. Only one sixth of the second layer of the PXD was installed for the data analyzed here. Outside the CDC is a time-of-propagation counter (TOP) [30] in the central region and an aerogel-based ring-imaging Cherenkov counter (ARICH) in the forward region. Surrounding the TOP and ARICH is the ECL and the 1.5 T superconducting solenoid magnet previously used in Belle. The magnet's flux return is instrumented with resistive-plate chambers and plastic scintillator modules to detect muons, K_L^0 mesons, and neutrons. More details on the Belle II detector are provided in ref. [25]. The symmetry axis of both Belle and Belle II detectors is defined as the z axis, and in both cases it is almost coincident with the electron beam direction. Both magnetic fields run parallel to the z axis.

This analysis uses both Belle and Belle II data sets, 980 fb $^{-1}$ recorded by Belle [24] and 428 fb $^{-1}$ recorded by Belle II [31]. The majority of the data (73% for Belle, 85% for Belle II) were recorded at an e^+e^- center-of-mass (c.m.) energy corresponding to the $\Upsilon(4S)$ resonance. The remaining data were recorded at energies slightly above and below the $\Upsilon(4S)$ resonance and at other $\Upsilon(nS)$ ($n = 1, 2, 3, 5$) resonances. The analysis is performed using the Belle II analysis software framework (BASF2) [32], with Belle data converted to BASF2 format with the B2BII software package [33]. We use Monte Carlo (MC) simulated events to optimize selection criteria, study backgrounds, and calculate reconstruction efficiencies. The MC samples are generated using EVTGEN [34], and the detector response

is simulated using GEANT3 [34] for Belle and GEANT4 [35] for Belle II. The continuum process $e^+e^- \rightarrow q\bar{q}$, where $q = u, d, s, c$, is generated using PYTHIA6 [36] for Belle and PYTHIA8 [37] and KKMC [38] for Belle II. Final-state radiation of charged particles is simulated with PHOTOS [39].

4 Event selection

Event selection criteria are chosen to maximize a figure-of-merit $\text{FOM} = N_S/\sqrt{N_S + N_B}$, where N_S is the signal yield expected in a region $|M(D) - m_D| < 13 \text{ MeV}/c^2$, and N_B is the background yield expected in this region. Here, $M(D) = M(K_S^0 K^- \pi^+ \pi^+)$ is the invariant mass of the $D_{(s)}^+$ candidate, m_D is the nominal $D_{(s)}^+$ mass [40], and the range corresponds to about 2.5σ in resolution. The background yield in the signal region is obtained from MC simulation and scaled by the ratio of yields between data and simulation in the sideband $20 \text{ MeV}/c^2 < |M(D) - m_D| < 40 \text{ MeV}/c^2$.

We require that signal candidates pass the following selection criteria: charged tracks must lie within the CDC acceptance (an angular coverage of $17^\circ \leq \theta \leq 150^\circ$), have at least one CDC hit, and have a distance-of-closest-approach to the e^+e^- interaction point (IP) of less than 2.0 cm along the z direction and of less than 0.5 cm in the x - y (transverse) plane. For each track, we calculate particle identification likelihoods (\mathcal{L}) for π and K particle hypotheses using information from the CDC, ACC, and TOF detectors in Belle, and mainly from the CDC, TOP, and ARICH detectors in Belle II. Tracks satisfying a likelihood ratio $\mathcal{L}_\pi/(\mathcal{L}_\pi + \mathcal{L}_K) > 0.6$ are identified as pions, and tracks satisfying a ratio $\mathcal{L}_K/(\mathcal{L}_K + \mathcal{L}_\pi) > 0.6$ are identified as kaons. Tracks that have high electron or muon likelihoods are rejected, where these lepton likelihoods are determined using information mainly from the ECL and KLM detectors, respectively [41–43]. All these requirements have an average efficiency of 91% for kaons and 95% for pions at Belle, and 87% for kaons and 90% for pions at Belle II.

Candidate K_S^0 mesons are reconstructed from pairs of oppositely-charged tracks assumed to be pions. To suppress non- K_S^0 background at Belle, a neural network (NN) [44] is employed. This NN uses 13 input variables [45]; the most discriminating are the K_S^0 momentum in the laboratory frame, the distance to the IP in the x - y plane for each track, and the K_S^0 flight length in the x - y plane. To suppress non- K_S^0 background at Belle II, the pion candidates are required to originate from a common vertex with a fit quality $\chi_{K_S^0}^2 < 100$. The invariant mass of the $K_S^0 \rightarrow \pi^+\pi^-$ candidate is required to lie within $10 \text{ MeV}/c^2$ of the nominal K_S^0 mass [40]. These requirements retain about 97% (Belle) and 92% (Belle II) of K_S^0 decays while rejecting more than 98% of non- K_S^0 background such as $D^+ \rightarrow K^- \pi^+ \pi^- \pi^+ \pi^-$.

We reconstruct $D_{(s)}^+$ candidates by combining a K_S^0 candidate, a K^- track, and two π^+ tracks. A vertex fitting algorithm [46] is applied to the entire decay chain, subject to a mass constraint for the K_S^0 and a constraint that the $D_{(s)}^+$ momentum originate from the IP. The resulting goodness-of-fit χ^2 is required to be less than 30 for D^+ decays and less than 40 for D_s^+ decays. The $D_{(s)}^+$ flight significance, defined as L_D/σ_{L_D} , is required to be greater than 3.0 (0.5) for D^+ (D_s^+) decays at Belle, and greater than 4.5 (2.0) for D^+ (D_s^+) decays at Belle II. Although the Belle II criteria are tighter, both sets of criteria have

similar efficiencies as a consequence of the superior vertex resolution of the Belle II PXD detector and significantly higher background rejection.

After the $D_{(s)}^+$ reconstruction, the K_S^0 flight length (L) is calculated as the projection of the displacement vector joining the $D_{(s)}^+$ and K_S^0 decay vertices onto the direction of the K_S^0 momentum. The uncertainty σ_L is calculated by propagating the uncertainties on the vertex positions and the K_S^0 momentum, accounting for their correlations. The K_S^0 flight significance L/σ_L is required to be greater than a minimum value, which is optimized separately for Belle and Belle II (greater than 10 at Belle and greater than 20 at Belle II).

We define a scaled momentum for the $D_{(s)}^+$ candidate as $x_p \equiv p_D/p_{\max}$, where p_D is the D momentum and $p_{\max} = \sqrt{E_{\text{beam}}^2 - M(D)^2 c^4}/c$. Here, E_{beam} is the beam energy, and both E_{beam} and p_D are evaluated in the e^+e^- center-of-mass frame. To suppress $D_{(s)}^+$ decays originating from B decays and also combinatorial background, we require $x_p > 0.5$. We also require that the invariant mass of the $D_{(s)}^+$ candidate satisfy $[M(D) - m_D] \in (-50, 40)$ MeV/ c^2 . For D_s^+ candidates, an additional background arising from $D^{*+} \rightarrow D^0(\rightarrow K_S^0 K^- \pi^+) \pi^+$ is present in the upper $M(K_S^0 K^- \pi^+ \pi^+)$ sideband. To suppress this background, we require that, for each π^+ candidate, $[M(K_S^0 K^- \pi^+ \pi^+) - M(K_S^0 K^- \pi^+)] > 151.57$ MeV/ c^2 . This requirement eliminates essentially all such background while preserving more than 99% of signal D_s^+ decays. The overall reconstruction efficiencies at Belle are 6% for D^+ decays and 9% for D_s^+ decays; the efficiencies at Belle II are very similar: 7% for D^+ decays and 9% for D_s^+ decays.

5 \mathcal{A}_{CP}^X measurement

We measure the asymmetries \mathcal{A}_{CP}^X , separately for Belle and Belle II, in two steps. We first perform a fit to the $M(D)$ distributions of a combined sample of $(D^+ + D^-)$ decays, and a combined sample of $(D_s^+ + D_s^-)$ decays. From this fit we determine the shape of the $M(D)$ probability density function (PDF) for signal decays. We subsequently perform a second fit for the asymmetries \mathcal{A}_{CP}^X , where the PDF shape for signal decays is fixed to that obtained from the first fit.

The PDF for signal is taken to be the sum of a double Gaussian and two (for D^+) or three (for D_s^+) asymmetric Gaussians. These functions share a common mean parameter but have distinct width parameters. All parameters, including the relative fractions of the Gaussians, are taken from MC simulation. However, a shift δ_μ to the mean and a common scaling factor k_σ for the widths are floated in the first fit (separately for D^+ and D_s^+) to account for small differences between data and MC simulation. For background, the PDF is taken to be a straight line, which over the range of interest describes the data well. The fitted $M(D)$ distributions and projections of the first fit result are shown in figure 3. The resulting signal and background yields in a window ± 10 MeV/ c^2 around the nominal $D_{(s)}^+$ mass [40] are listed in table 1. The ratio of signal to background for Belle II is higher than that for Belle due to the improved resolution on the $D_{(s)}^+$ mass and flight length L_D .

For the second fit to determine \mathcal{A}_{CP}^X , the data is divided into four subsamples as determined by the charge of $D_{(s)}^\pm$ and the sign of X . For all subsamples, the background slope

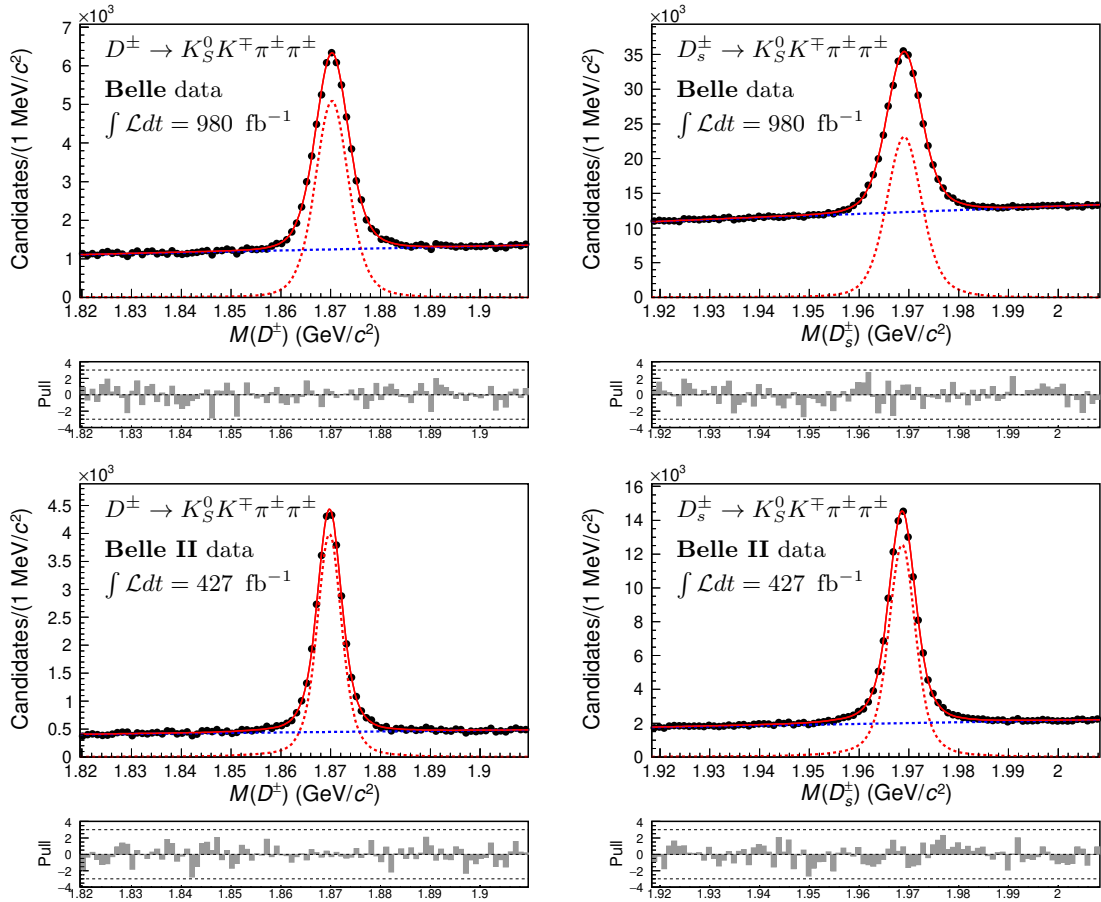


Figure 3. Invariant mass distributions for $D_{(s)}^{\pm} \rightarrow K_S^0 K^{\mp} \pi^{\pm} \pi^{\pm}$ candidates (points with error bars), with fit results overlaid. The red dashed curves show the fitted signal, and the blue dash-dotted curves show the fitted background. The top plots show Belle data, and the bottom plots show Belle II data. The smaller panels show the pull distributions, where the pull is defined as $(\text{data yield} - \text{fitted yield}) / (\text{data uncertainty})$.

Table 1. Fitted signal and background yields in a window $\pm 10 \text{ MeV}/c^2$ around the nominal $D_{(s)}^{\pm}$ mass [40]. The uncertainties listed are statistical.

Component	$D^{\pm} \rightarrow K_S^0 K^{\mp} \pi^{\pm} \pi^{\pm}$		$D_s^{\pm} \rightarrow K_S^0 K^{\mp} \pi^{\pm} \pi^{\pm}$	
	Belle	Belle II	Belle	Belle II
Signal (N_{sig})	44048 ± 288	26738 ± 199	210743 ± 780	92000 ± 393
Background (N_{bkg})	24844 ± 88	8964 ± 53	245285 ± 280	39997 ± 114
Ratio ($N_{\text{sig}}/N_{\text{bkg}}$)	1.8	3.0	0.9	2.3

and calibration factors δ_μ and k_σ are fixed to the values obtained from the first fit. The yields of the subsamples are expressed as:

$$N(D_{(s)}^+, X > 0) = \frac{N_+}{2}(1 + A_X) \quad (5.1)$$

$$N(D_{(s)}^+, X < 0) = \frac{N_+}{2}(1 - A_X) \quad (5.2)$$

$$N(D_{(s)}^-, \bar{X} > 0) = \frac{N_-}{2}(1 + A_X - 2\mathcal{A}_{CP}^X) \quad (5.3)$$

$$N(D_{(s)}^-, \bar{X} < 0) = \frac{N_-}{2}(1 - A_X + 2\mathcal{A}_{CP}^X). \quad (5.4)$$

Here, $N_+ = N(D_{(s)}^+, X > 0) + N(D_{(s)}^+, X < 0)$ and $N_- = N(D_{(s)}^-, \bar{X} > 0) + N(D_{(s)}^-, \bar{X} < 0)$ represent the total signal yields for $D_{(s)}^+$ and $D_{(s)}^-$, respectively; A_X denotes the asymmetry for X as defined in eq. 2.3; and \mathcal{A}_{CP}^X denotes the CP -violating parameter as defined in eq. 2.5. We perform a simultaneous fit to the $M(D)$ distributions of these four subsamples to extract parameters N_+ , N_- , A_X , and \mathcal{A}_{CP}^X . We test the fitting procedure on MC samples generated with different input values of \mathcal{A}_{CP}^X ; in all cases we obtain fitted values for \mathcal{A}_{CP}^X consistent with the input values.

The results for \mathcal{A}_{CP}^X are listed in table 2 along with systematic uncertainties. These uncertainties are discussed in the next section. The fitted $M(D)$ distributions are shown in appendix A. The Belle II distributions for C_{TP} and $-\bar{C}_{TP}$, and for C_{QP} and \bar{C}_{QP} , are shown in appendix B; the corresponding distributions for Belle look very similar. No difference in shapes is seen between $D_{(s)}^+$ and $D_{(s)}^-$ decays.

Table 2. Results for \mathcal{A}_{CP}^X in units of 10^{-3} for $D_{(s)}^+ \rightarrow K_S^0 K^- \pi^+ \pi^+$ decays. The first and second uncertainties listed are statistical and systematic, respectively. The last column lists the significance of the combined result from $\mathcal{A}_{CP}^X = 0$.

X	\mathcal{A}_{CP}^X Belle	\mathcal{A}_{CP}^X Belle II	Combined \mathcal{A}_{CP}^X	Significance	
D^+	C_{TP}	$-4.0 \pm 5.9 \pm 3.0$	$-0.2 \pm 7.0 \pm 1.8$	$-2.3 \pm 4.5 \pm 1.5$	0.5σ
	C_{QP}	$-1.0 \pm 5.9 \pm 2.5$	$-0.4 \pm 7.0 \pm 2.4$	$-0.7 \pm 4.5 \pm 1.7$	0.2σ
	$C_{TP} C_{QP}$	$+6.4 \pm 5.9 \pm 2.2$	$+0.6 \pm 7.0 \pm 1.3$	$+3.9 \pm 4.5 \pm 1.1$	0.8σ
	$\cos\theta_{K_S^0} \cos\theta_{K^-}$	$-4.7 \pm 5.9 \pm 3.0$	$-0.6 \pm 6.9 \pm 3.0$	$-2.9 \pm 4.5 \pm 2.1$	0.6σ
	$C_{TP} \cos\theta_{K_S^0} \cos\theta_{K^-}$	$+1.9 \pm 5.9 \pm 2.0$	$-0.2 \pm 7.0 \pm 1.9$	$+1.0 \pm 4.5 \pm 1.4$	0.2σ
	$C_{QP} \cos\theta_{K_S^0} \cos\theta_{K^-}$	$+14.9 \pm 5.9 \pm 1.4$	$+7.0 \pm 7.0 \pm 1.6$	$+11.6 \pm 4.5 \pm 1.1$	2.5σ
D_s^+	C_{TP}	$-0.3 \pm 3.1 \pm 1.3$	$+1.0 \pm 3.9 \pm 1.1$	$+0.2 \pm 2.4 \pm 0.8$	0.1σ
	C_{QP}	$+0.6 \pm 3.1 \pm 1.2$	$+2.0 \pm 3.9 \pm 1.4$	$+1.1 \pm 2.4 \pm 0.9$	0.4σ
	$C_{TP} C_{QP}$	$+1.5 \pm 3.2 \pm 1.4$	$-2.7 \pm 3.9 \pm 1.7$	$-0.2 \pm 2.5 \pm 1.1$	0.1σ
	$\cos\theta_{K_S^0} \cos\theta_{K^-}$	$-3.7 \pm 3.1 \pm 1.1$	$-6.3 \pm 3.9 \pm 1.2$	$-4.7 \pm 2.4 \pm 0.8$	1.8σ
	$C_{TP} \cos\theta_{K_S^0} \cos\theta_{K^-}$	$-4.4 \pm 3.2 \pm 1.4$	$+0.8 \pm 3.9 \pm 1.4$	$-2.2 \pm 2.5 \pm 1.0$	0.8σ
	$C_{QP} \cos\theta_{K_S^0} \cos\theta_{K^-}$	$-1.6 \pm 3.1 \pm 1.3$	$-0.0 \pm 3.9 \pm 1.7$	$-1.0 \pm 2.4 \pm 1.0$	0.4σ

6 Systematic uncertainties

Many systematic uncertainties for the measurements of X and \bar{X} cancel in the ratios A_X (eq. 2.3) and $A_{\bar{X}}$ (eq. 2.4), or in the difference between them (eq. 2.5). The uncertainties that do not cancel are listed in table 3 and discussed below.

Table 3. Systematic uncertainties (absolute) for \mathcal{A}_{CP}^X in units of 10^{-3} in $D_{(s)}^+ \rightarrow K_S^0 K^- \pi^+ \pi^+$ decays, where $X = C_{TP}$ (1), C_{QP} (2), $C_{TP}C_{QP}$ (3), $\cos \theta_{K_S^0} \cos \theta_{K^-}$ (4), $C_{TP} \cos \theta_{K_S^0} \cos \theta_{K^-}$ (5), and $C_{QP} \cos \theta_{K_S^0} \cos \theta_{K^-}$ (6).

Source	$D^+ \rightarrow K_S^0 K^- \pi^+ \pi^+$ at Belle						$D^+ \rightarrow K_S^0 K^- \pi^+ \pi^+$ at Belle II					
	(1)	(2)	(3)	(4)	(5)	(6)	(1)	(2)	(3)	(4)	(5)	(6)
X -dependent efficiency	3.0	2.4	1.9	2.8	1.8	1.4	1.2	2.4	1.1	2.6	1.5	1.3
X -resolution asymmetry	0.2	0.7	0.4	0.7	0.6	0.3	0.7	0.1	0.1	0.9	0.2	0.7
Signal/background PDF	0.0	0.0	0.0	0.0	0.0	0.0	0.0	0.0	0.0	0.0	0.0	0.0
Simultaneous fit bias	0.2	0.2	0.1	0.2	0.1	0.2	0.2	0.2	0.2	0.1	0.2	0.2
D_s^+ feeddown background	0.4	0.3	1.0	0.7	0.1	0.2	1.1	0.4	0.6	1.1	1.2	0.6
Total σ_{syst}	3.0	2.5	2.2	3.0	2.0	1.4	1.8	2.4	1.3	3.0	1.9	1.6

Source	$D_s^+ \rightarrow K_S^0 K^- \pi^+ \pi^+$ at Belle						$D_s^+ \rightarrow K_S^0 K^- \pi^+ \pi^+$ at Belle II					
	(1)	(2)	(3)	(4)	(5)	(6)	(1)	(2)	(3)	(4)	(5)	(6)
X -dependent efficiency	1.2	1.1	1.4	1.1	1.2	1.3	1.1	1.4	1.7	1.2	1.4	1.6
X -resolution asymmetry	0.6	0.5	0.1	0.2	0.8	0.3	0.2	0.1	0.2	0.0	0.2	0.4
Signal/background PDF	0.0	0.0	0.0	0.0	0.0	0.0	0.0	0.0	0.0	0.0	0.0	0.0
Simultaneous fit bias	0.1	0.0	0.0	0.1	0.1	0.0	0.1	0.2	0.2	0.3	0.2	0.2
Total σ_{syst}	1.3	1.2	1.4	1.1	1.4	1.3	1.1	1.4	1.7	1.2	1.4	1.7

A difference in efficiencies between positive and negative X values could lead to false asymmetries A_X and $A_{\bar{X}}$. Such a difference is evaluated using MC simulation by comparing reconstructed X distributions with those that were generated. For $X = C_{TP}$ and $C_{TP}C_{QP}$, no significant X -dependence is observed. For the other observables, a small dependence is observed, but it is the same for $D_{(s)}^+$ and $D_{(s)}^-$ decays and thus the effect upon \mathcal{A}_{CP}^X is small. To account for this quantitatively, we take as a systematic uncertainty the difference between generated and reconstructed values of \mathcal{A}_{CP}^X . We include in this uncertainty the statistical uncertainty of the MC samples used. Finally, we include in this uncertainty any effect upon \mathcal{A}_{CP}^X arising from a possible difference between MC simulation and data for X -dependent efficiencies. We evaluate this as follows. The asymmetry in detection efficiencies between K^+ and K^- (denoted A_ϵ^K) is measured in data as a function of momentum and polar angle using $D^0 \rightarrow K^- \pi^+$ and $D_s^+ \rightarrow \phi \pi^+$ decays [47], and the asymmetry in detection efficiencies between π^+ and π^- (denoted A_ϵ^π) is measured using $D^+ \rightarrow K^- \pi^+ \pi^+$ and $D^0 \rightarrow K^- \pi^+ \pi^0$ decays [48]. We scale MC signal events with weighting factors based on these asymmetries and repeat the fits for \mathcal{A}_{CP}^X . For $D_{(s)}^+ \rightarrow K_S^0 K^- \pi^+ \pi^+$, the weighting factor is $(1 - A_\epsilon^K)(1 + A_\epsilon^\pi)(1 + A_\epsilon^\pi)$; for $D_{(s)}^- \rightarrow K_S^0 K^+ \pi^- \pi^-$, the weighting factor is $(1 + A_\epsilon^K)(1 - A_\epsilon^\pi)(1 - A_\epsilon^\pi)$. After fitting these reweighted events, the resulting change in \mathcal{A}_{CP}^X is included in the systematic uncertainty for X -dependent efficiency. This contribution

is very small ($< 5 \times 10^{-4}$).

We consider the effect of a difference in X resolution between positive and negative values. If such a difference existed, then a different number of events could shift from $-X$ to $+X$ values than from $+X$ to $-X$, corrupting the A_X measurement. From MC simulation, we find that the net fraction of signal decays changing sign in X is very small, less than 0.1%. To evaluate the effect quantitatively, we study the X resolution for different ranges of X . We find the resolution in X to depend on X but be well-described by a parabola symmetric about $X = 0$. The statistical error on this parabola is used to generate MC samples with asymmetric resolution; these samples are then fitted and the resulting change in \mathcal{A}_{CP}^X is taken as the systematic uncertainty due to a possible asymmetry in X resolution.

The uncertainty due to fixed PDF shape parameters is evaluated by varying these parameters by their uncertainties and repeating the fit. We sample all parameters simultaneously from Gaussian distributions having widths equal to their uncertainties, and repeat this sampling and subsequent fitting 1000 times. During this sampling, correlations among the sampled parameters are accounted for. The 1000 fitted values for \mathcal{A}_{CP}^X are recorded, and the standard deviation of this distribution is taken as the systematic uncertainty due to signal and background PDF shapes. These uncertainties are very small, less than 2×10^{-5} .

To assess any bias in our fitting procedure, we fit a large sample of “toy” MC events generated by sampling the PDFs used to fit the data. The number of generated events for $\pm X$ and $\pm \bar{X}$ vary: they are calculated for different input values of \mathcal{A}_{CP}^X , which range from -0.015 to 0.015 . For each input value, an ensemble of MC events is generated. These ensembles are fitted, and the mean value of the \mathcal{A}_{CP}^X results is calculated. Plotting these mean values against the input values shows a linear dependence. Fitting these points to a line gives a slope consistent with unity and an intercept consistent with zero. We assign the difference between our measured value and the corresponding input value as given by the fitted line as a systematic uncertainty due to possible fit bias. The uncertainty on the difference is included in this calculation.

For the $D^+ \rightarrow K_S^0 K^- \pi^+ \pi^+$ decay mode, we consider the effect of possible background from $D_s^+ \rightarrow K_S^0 K^- \pi^+ \pi^+ \pi^0$, with the π^0 missed. This five-body decay is unmeasured, and thus to evaluate the effect of this background, we include a component for it in our fit. We take the shape of its PDF from MC simulation and float its yield. The difference between the resulting value of \mathcal{A}_{CP}^X and our nominal result is taken as a systematic uncertainty.

Combining all systematic uncertainties in quadrature gives the total systematic uncertainties listed in table 3. These total uncertainties are also included in table 2. For all \mathcal{A}_{CP}^X measurements, the total systematic uncertainties are notably less than the corresponding statistical uncertainties.

7 Combined result and summary

Table 2 lists our results for the six asymmetries \mathcal{A}_{CP}^X , for both Belle and Belle II. We combine the results from the two data sets using the formulae

$$\mathcal{A}_{CP}^X = \frac{\mathcal{A}_{CP}^{B1}/\sigma_{B1}^2 + \mathcal{A}_{CP}^{B2}/\sigma_{B2}^2}{1/\sigma_{B1}^2 + 1/\sigma_{B2}^2} \quad (7.1)$$

$$\sigma_{\mathcal{A}_{CP}^X} = 1/\sqrt{1/\sigma_{B1}^2 + 1/\sigma_{B2}^2}, \quad (7.2)$$

where σ_{B1} and σ_{B2} represent the total uncertainties (sum in quadrature of statistical and systematic uncertainties) for Belle and Belle II measurements, respectively. The combined results are also listed in table 2; the resulting uncertainties are at the level of 0.5% for D^+ decays and better than 0.3% for D_s^+ decays. We calculate the significances of the combined results from $\mathcal{A}_{CP}^X = 0$ by dividing the central values by their total uncertainties. These significances are listed in the right-most column of table 2 and are mostly less than 1σ . The largest significance (for D^+ , $X = C_{QP} \cos \theta_{K_S^0} \cos \theta_{K^-}$) is 2.5σ , which is plausible as a statistical fluctuation.

In summary, we have performed the first search for CP violation in four-body $D_{(s)}^+ \rightarrow K_S^0 K^- \pi^+ \pi^+$ decays using triple and quadruple products. We use both Belle and Belle II datasets corresponding to a total integrated luminosity of 1408 fb^{-1} . We have measured CP asymmetries for six different observables consisting of the triple product C_{TP} , the quadruple product C_{QP} , the product $C_{TP}C_{QP}$, the product of the cosines of helicity angles $\theta_{K_S^0}$ and θ_{K^-} , and the products of C_{TP} and C_{QP} with the product $\cos \theta_{K_S^0} \cos \theta_{K^-}$. All results are listed in table 2. No evidence for CP violation is found. These results represent the world's most precise measurements of the triple-product asymmetry for D_s^+ decays and for singly Cabibbo-suppressed D^+ decays, and the first use of the other \mathcal{A}_{CP}^X asymmetries to search for CP violation in the charm sector.

A Simultaneously fitted distributions for $D_{(s)}^+$ data

The $M(D)$ distributions for $D_{(s)}^+ \rightarrow K_S^0 K^\mp \pi^\pm \pi^\pm$ decays used to fit for the asymmetries \mathcal{A}_{CP}^X , with fit results overlaid, are shown in figs. 4-9. Specifically, fig. 4 corresponds to $X = C_{TP}$, fig. 5 to $X = C_{QP}$, fig. 6 to $X = C_{TP}C_{QP}$, fig. 7 to $X = \cos \theta_{K_S^0} \cos \theta_{K^-}$, fig. 8 to $X = C_{TP} \cos \theta_{K_S^0} \cos \theta_{K^-}$, and fig. 9 to $X = C_{QP} \cos \theta_{K_S^0} \cos \theta_{K^-}$.

B Triple- and quadruple-product distributions

The Belle II distributions of the triple product C_{TP} and quadruple product C_{QP} for $D_{(s)}^+ \rightarrow K_S^0 K^- \pi^+ \pi^+$ candidates, and $-\overline{C}_{TP}$ and \overline{C}_{QP} for $D_{(s)}^- \rightarrow K_S^0 K^+ \pi^- \pi^-$ candidates, are shown in fig. 10.

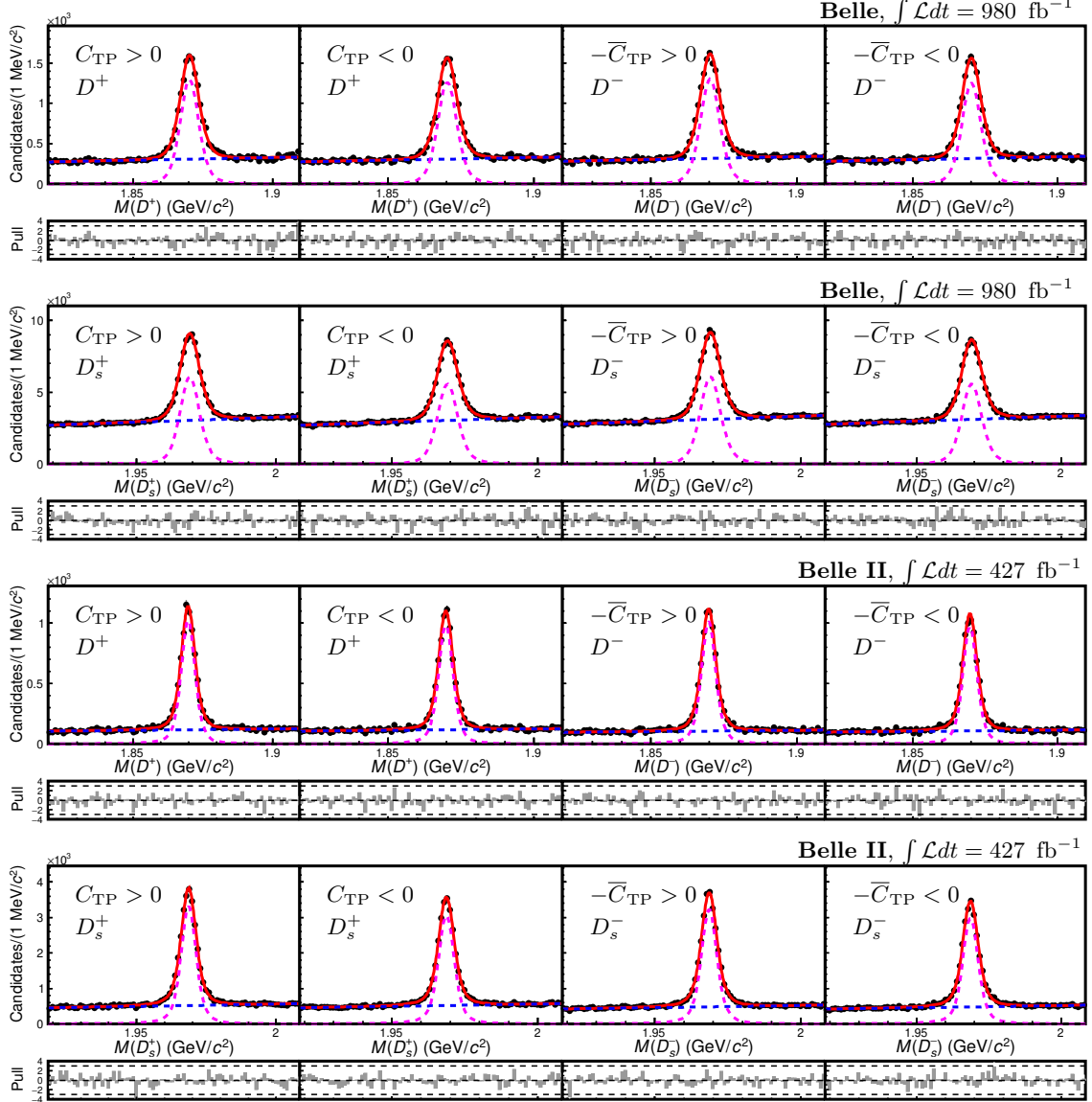


Figure 4. Fitted distributions of $D_{(s)}^{\pm} \rightarrow K_S^0 K^{\mp} \pi^{\pm} \pi^{\pm}$ data at Belle (top two rows) and Belle II (bottom two rows), for the triple product C_{TP} . The red dashed curves show the fitted signal, and the blue dash-dotted curves show the fitted background. The smaller panels show the pull distributions.

Acknowledgments

This work, based on data collected using the Belle II detector, which was built and commissioned prior to March 2019, and data collected using the Belle detector, which was operated until June 2010, was supported by Higher Education and Science Committee of the Republic of Armenia Grant No. 23LCG-1C011; Australian Research Council and Research Grants No. DP200101792, No. DP210101900, No. DP210102831, No. DE220100462, No. LE210100098, and No. LE230100085; Austrian Federal Ministry of Education, Science and Research, Austrian Science Fund No. P 34529, No. J 4731, No. J 4625, and No. M 3153,

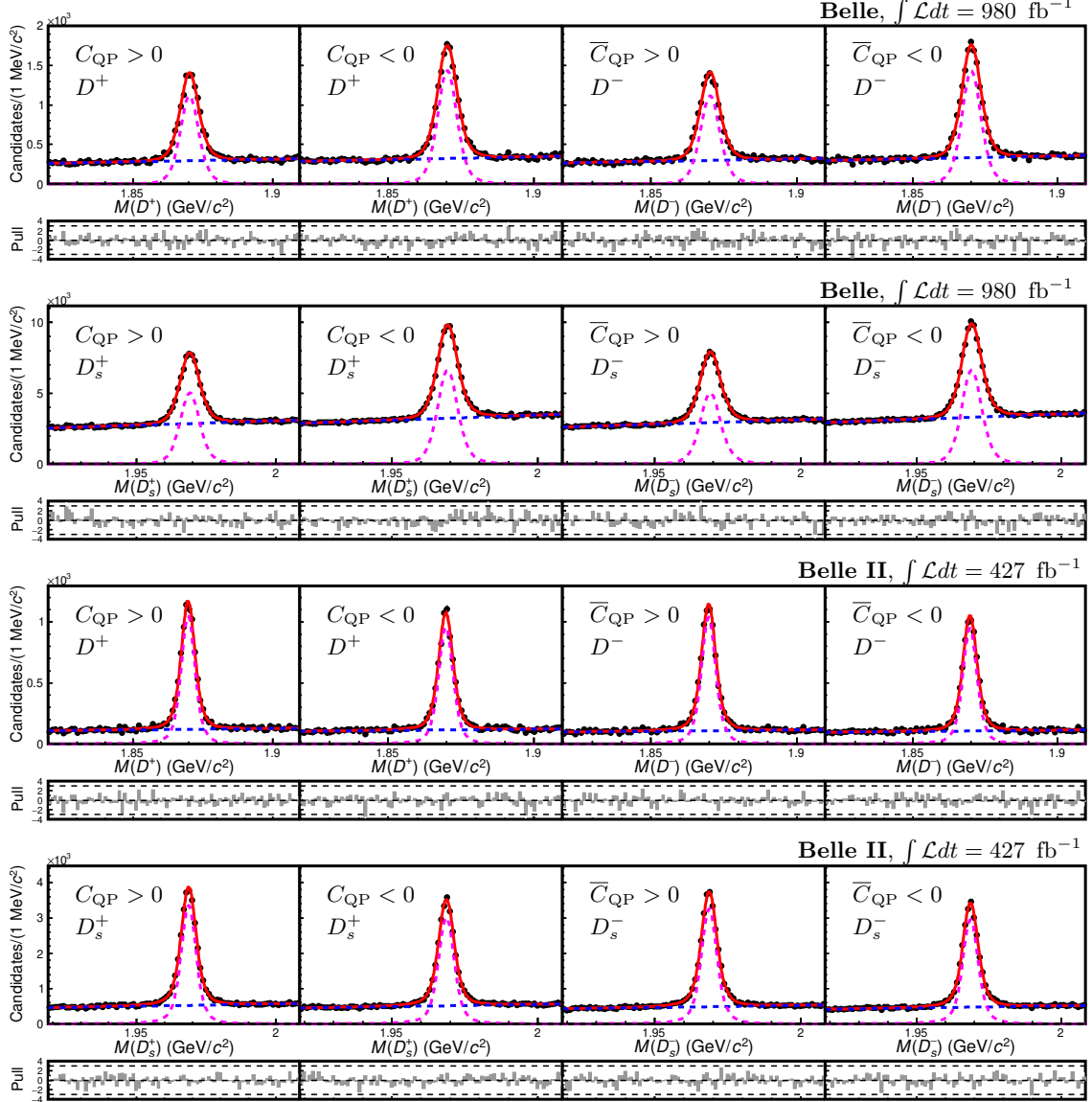


Figure 5. Fitted distributions of $D_{(s)}^{\pm} \rightarrow K_S^0 K^{\mp} \pi^{\pm} \pi^{\pm}$ data at Belle (top two rows) and Belle II (bottom two rows), for the quadruple product C_{QP} . The red dashed curves show the fitted signal, and the blue dash-dotted curves show the fitted background. The smaller panels show the pull distributions.

and Horizon 2020 ERC Starting Grant No. 947006 “InterLeptons”; Natural Sciences and Engineering Research Council of Canada, Compute Canada and CANARIE; National Key R&D Program of China under Contract No. 2022YFA1601903, National Natural Science Foundation of China and Research Grants No. 11575017, No. 11761141009, No. 11705209, No. 11975076, No. 12135005, No. 12150004, No. 12161141008, and No. 12175041, and Shandong Provincial Natural Science Foundation Project ZR2022JQ02; the Czech Science Foundation Grant No. 22-18469S and Charles University Grant Agency project No. 246122; European Research Council, Seventh Framework PIFI-GA-2013-622527, Horizon 2020 ERC-

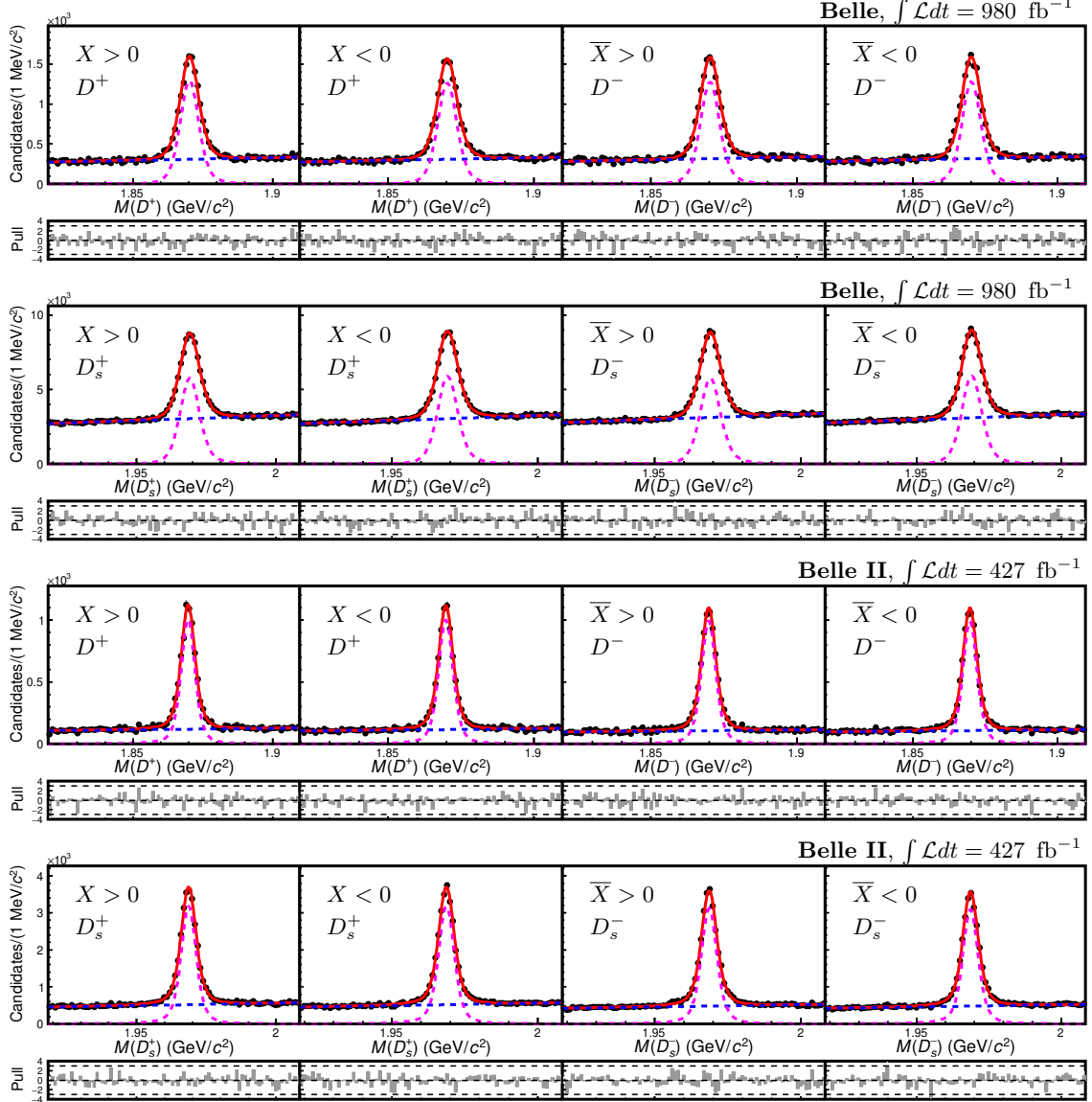


Figure 6. Fitted distributions of $D_{(s)}^{\pm} \rightarrow K_S^0 K^{\mp} \pi^{\pm} \pi^{\pm}$ data at Belle (top two rows) and Belle II (bottom two rows) for $X = C_{\text{TP}} C_{\text{QP}}$. The red dashed curves show the fitted signal, and the blue dash-dotted curves show the fitted background. The smaller panels show the pull distributions.

Advanced Grants No. 267104 and No. 884719, Horizon 2020 ERC-Consolidator Grant No. 819127, Horizon 2020 Marie Skłodowska-Curie Grant Agreement No. 700525 “NIOBE” and No. 101026516, and Horizon 2020 Marie Skłodowska-Curie RISE project JENNIFER2 Grant Agreement No. 822070 (European grants); L’Institut National de Physique Nucléaire et de Physique des Particules (IN2P3) du CNRS and L’Agence Nationale de la Recherche (ANR) under grant ANR-21-CE31-0009 (France); BMBF, DFG, HGF, MPG, and AvH Foundation (Germany); Department of Atomic Energy under Project Identification No. RTI 4002, Department of Science and Technology, and UPES SEED funding programs No. UPES/R&D-SEED-INFRA/17052023/01 and No. UPES/R&D-SOE/20062022/06

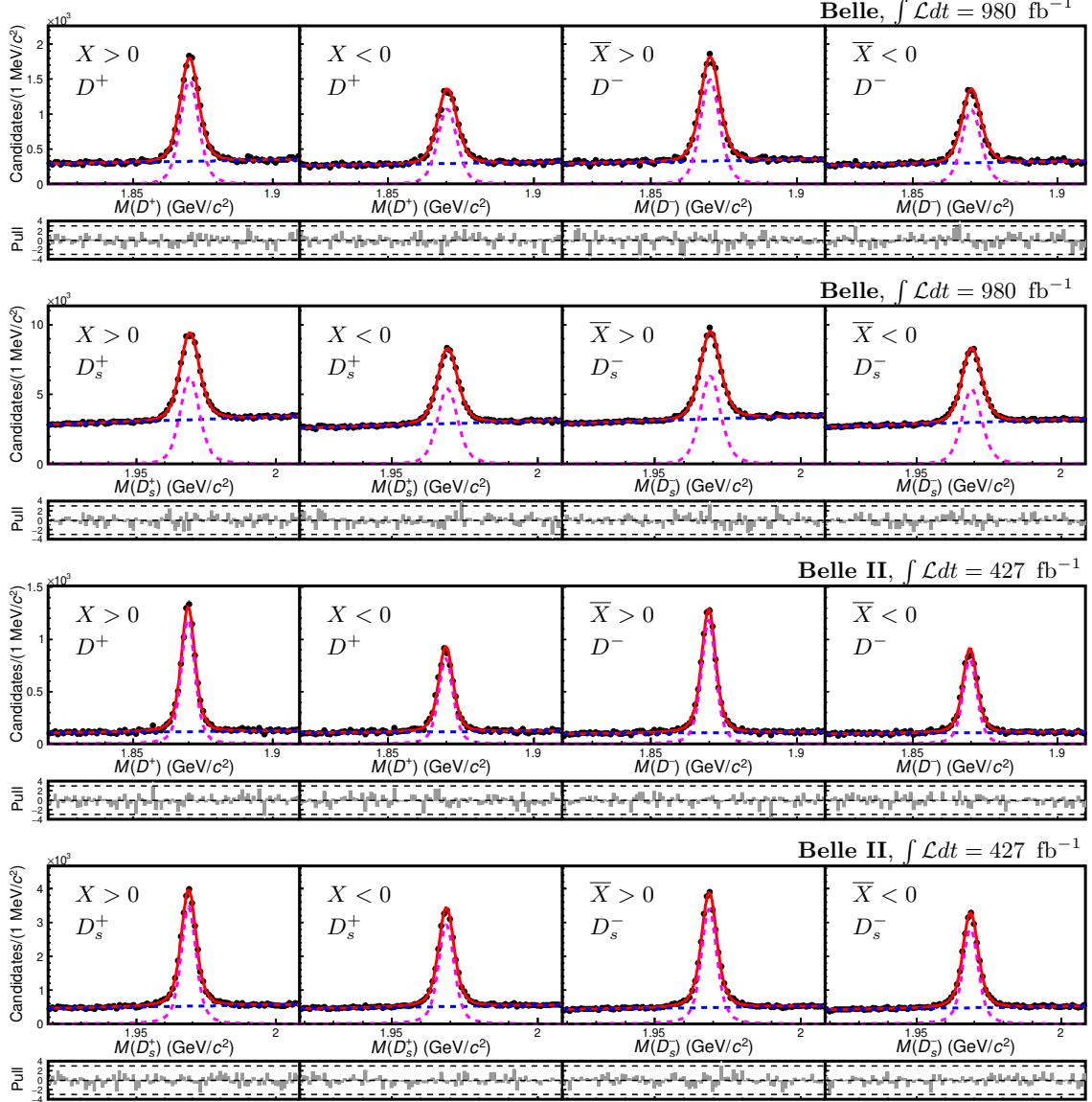


Figure 7. Fitted distributions of $D_{(s)}^{\pm} \rightarrow K_S^0 K^{\mp} \pi^{\pm} \pi^{\pm}$ data at Belle (top two rows) and Belle II (bottom two rows) for $X = \cos \theta_{K_S^0} \cos \theta_{K^-}$. The red dashed curves show the fitted signal, and the blue dash-dotted curves show the fitted background. The smaller panels show the pull distributions.

(India); Israel Science Foundation Grant No. 2476/17, U.S.-Israel Binational Science Foundation Grant No. 2016113, and Israel Ministry of Science Grant No. 3-16543; Istituto Nazionale di Fisica Nucleare and the Research Grants BELLE2; Japan Society for the Promotion of Science, Grant-in-Aid for Scientific Research Grants No. 16H03968, No. 16H03993, No. 16H06492, No. 16K05323, No. 17H01133, No. 17H05405, No. 18K03621, No. 18H03710, No. 18H05226, No. 19H00682, No. 20H05850, No. 20H05858, No. 22H00144, No. 22K14056, No. 22K21347, No. 23H05433, No. 26220706, and No. 26400255, and the Ministry of Education, Culture, Sports, Science, and Technology (MEXT) of Japan; National Research Foundation (NRF) of Korea Grants No. 2016R1-D1A1B-02012900, No. 2018R1-

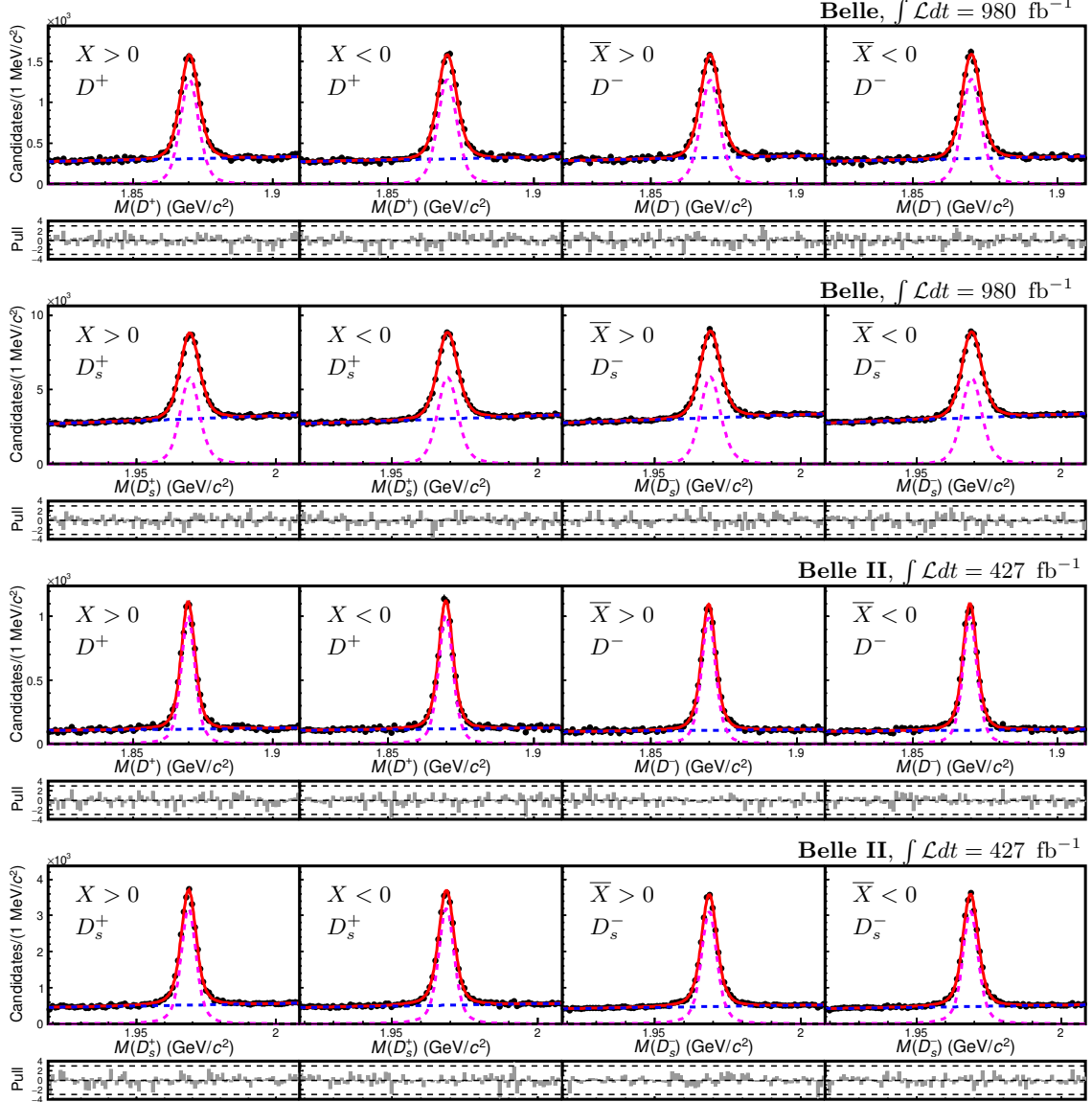


Figure 8. Fitted distributions of $D^\pm \rightarrow K_S^0 K^\mp \pi^\pm \pi^\pm$ data at Belle (top two rows) and Belle II (bottom two rows) for $X = C_{\text{TP}} \cos \theta_{K_S^0} \cos \theta_{K^-}$. The red dashed curves show the fitted signal, and the blue dash-dotted curves show the fitted background. The smaller panels show the pull distributions.

A6A1A-06024970, No. 2021R1-A6A1A-03043957, No. 2021R1-F1A-1060423, No. 2021R1-F1A-1064008, No. 2022R1-A2C-1003993, No. 2022R1-A2C-1092335, No. RS-2023-00208693, No. RS-2024-00354342 and No. RS-2022-00197659, Radiation Science Research Institute, Foreign Large-Size Research Facility Application Supporting project, the Global Science Experimental Data Hub Center, the Korea Institute of Science and Technology Information (K24L2M1C4) and KREONET/GLORIAD; Universiti Malaya RU grant, Akademi Sains Malaysia, and Ministry of Education Malaysia; Frontiers of Science Program Contracts No. FOINS-296, No. CB-221329, No. CB-236394, No. CB-254409, and No. CB-

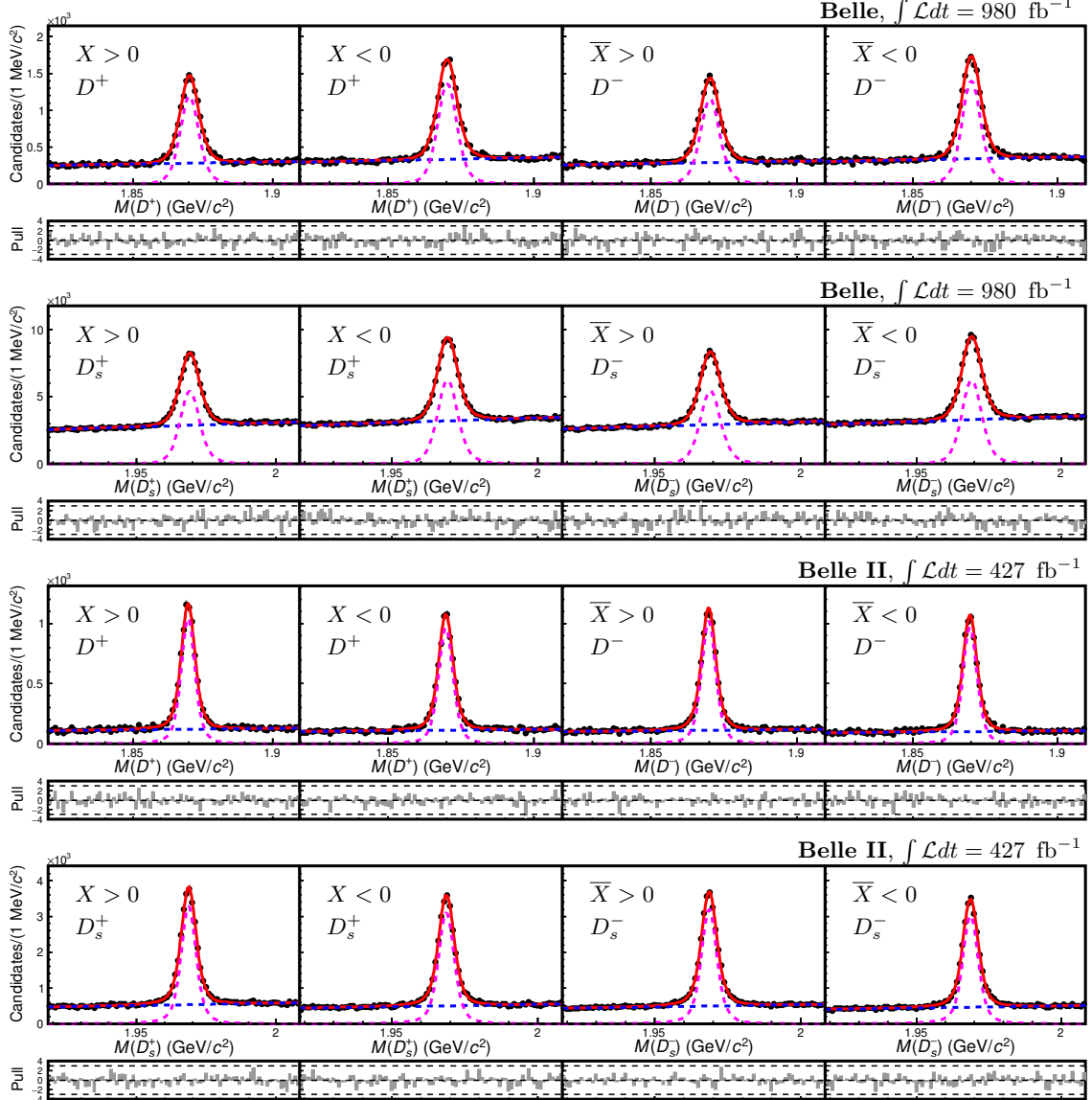


Figure 9. Fitted distributions of $D^\pm \rightarrow K_S^0 K^\mp \pi^\pm \pi^\pm$ data at Belle (top two rows) and Belle II (bottom two rows) for $X = C_{\text{QP}} \cos \theta_{K_S^0} \cos \theta_{K^-}$. The red dashed curves show the fitted signal, and the blue dash-dotted curves show the fitted background. The smaller panels show the pull distributions.

180023, and SEP-CINVESTAV Research Grant No. 237 (Mexico); the Polish Ministry of Science and Higher Education and the National Science Center; the Ministry of Science and Higher Education of the Russian Federation and the HSE University Basic Research Program, Moscow; University of Tabuk Research Grants No. S-0256-1438 and No. S-0280-1439 (Saudi Arabia); Slovenian Research Agency and Research Grants No. J1-9124 and No. P1-0135; Ikerbasque, Basque Foundation for Science, the State Agency for Research of the Spanish Ministry of Science and Innovation through Grant No. PID2022-136510NB-C33, Agencia Estatal de Investigacion, Spain Grant No. RYC2020-029875-I and Generalitat

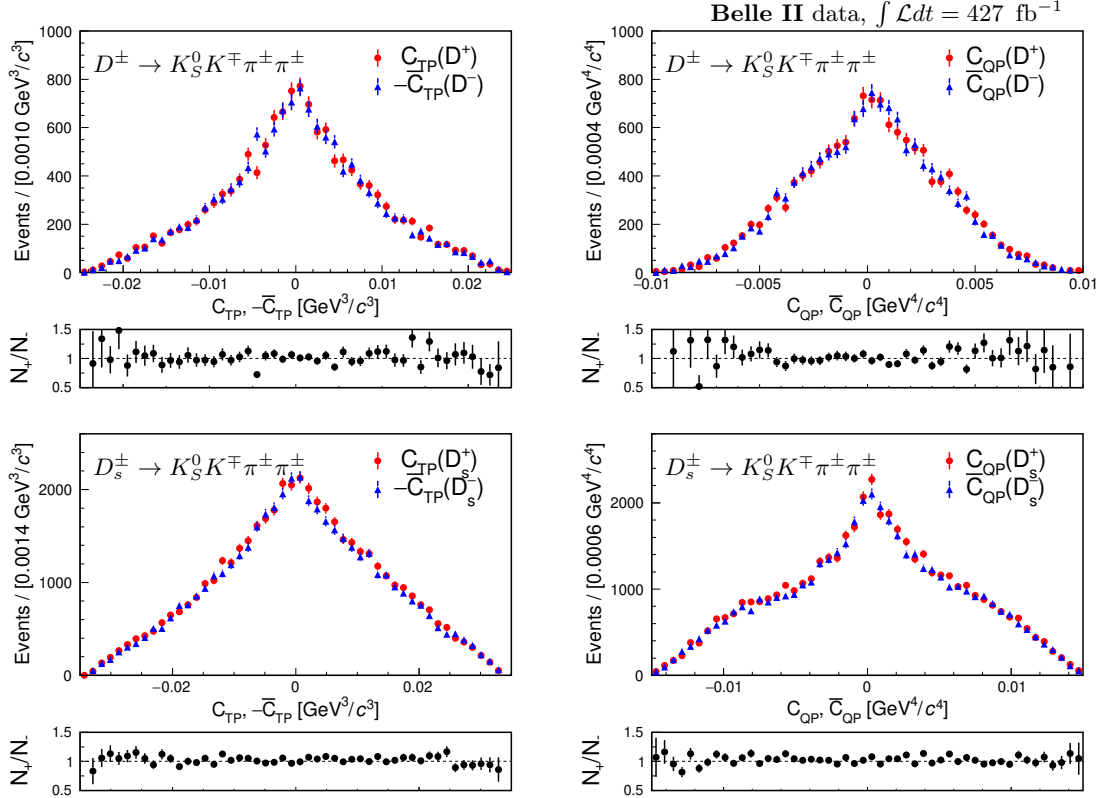


Figure 10. Belle II distributions for C_{TP} (left) and C_{QP} (right) for $D_{(s)}^+ \rightarrow K_S^0 K^- \pi^+ \pi^+$ candidates, and $-\overline{C}_{\text{TP}}$ (left) and \overline{C}_{QP} (right) for $D_{(s)}^- \rightarrow K_S^0 K^+ \pi^- \pi^-$ candidates. Points with error bars denote candidates in the signal region $|M(D) - m_D| < 10 \text{ MeV}/c^2$ after background (scaled from the sideband $20 \text{ MeV}/c^2 < |M(D) - m_D| < 40 \text{ MeV}/c^2$) has been subtracted. The lower panels show the ratios $C_{\text{TP}}/(-\overline{C}_{\text{TP}})$ and $C_{\text{QP}}/\overline{C}_{\text{QP}}$.

Valenciana, Spain Grant No. CIDEGENT/2018/020; the Swiss National Science Foundation; The Knut and Alice Wallenberg Foundation (Sweden), Contracts No. 2021.0174 and No. 2021.0299; National Science and Technology Council, and Ministry of Education (Taiwan); Thailand Center of Excellence in Physics; TUBITAK ULAKBIM (Turkey); National Research Foundation of Ukraine, Project No. 2020.02/0257, and Ministry of Education and Science of Ukraine; the U.S. National Science Foundation and Research Grants No. PHY-1913789 and No. PHY-2111604, and the U.S. Department of Energy and Research Awards No. DE-AC06-76RLO1830, No. DE-SC0007983, No. DE-SC0009824, No. DE-SC0009973, No. DE-SC0010007, No. DE-SC0010073, No. DE-SC0010118, No. DE-SC0010504, No. DE-SC0011784, No. DE-SC0012704, No. DE-SC0019230, No. DE-SC0021274, No. DE-SC0021616, No. DE-SC0022350, No. DE-SC0023470; and the Vietnam Academy of Science and Technology (VAST) under Grants No. NVCC.05.12/22-23 and No. DL0000.02/24-25.

These acknowledgements are not to be interpreted as an endorsement of any statement made by any of our institutes, funding agencies, governments, or their representatives.

We thank the SuperKEKB team for delivering high-luminosity collisions; the KEK

cryogenics group for the efficient operation of the detector solenoid magnet and IBelle on site; the KEK Computer Research Center for on-site computing support; the NII for SINET6 network support; and the raw-data centers hosted by BNL, DESY, GridKa, IN2P3, INFN, PNNL/EMSL, and the University of Victoria. We warmly thank Fu-Sheng Yu and Zhen-Hua Zhang for valuable and helpful discussions.

References

- [1] A.D. Sakharov, *Violation of CP Invariance, C asymmetry, and baryon asymmetry of the universe*, *Pisma Zh. Eksp. Teor. Fiz.* **5** (1967) 32.
- [2] M. Kobayashi and T. Maskawa, *CP violation in the renormalizable theory of weak interaction*, *Prog. Theor. Phys.* **49** (1973) 652.
- [3] J. Brod, A.L. Kagan and J. Zupan, *Size of direct CP violation in singly Cabibbo-suppressed D decays*, *Phys. Rev. D* **86** (2012) 014023 [[arXiv:1111.5000](#)].
- [4] H.-Y. Cheng and C.-W. Chiang, *Revisiting CP violation in $D \rightarrow PP$ and VP decays*, *Phys. Rev. D* **100** (2019) 093002 [[arXiv:1909.03063](#)].
- [5] H.-Y. Cheng and C.-W. Chiang, *CP violation in quasi-two-body $D \rightarrow VP$ decays and three-body D decays mediated by vector resonances*, *Phys. Rev. D* **104** (2021) 073003 [[arXiv:2104.13548](#)].
- [6] A. Dery and Y. Nir, *Implications of the LHCb discovery of CP violation in charm decays*, *JHEP* **12** (2019) 104 [[arXiv:1909.11242](#)].
- [7] D. Delepine, G. Faisel and C.A. Ramirez, *Direct CP violation in $D^+ \rightarrow K^0(\bar{K}^0)\pi^+$ decays as a probe for new physics*, *Eur. Phys. J. C* **80** (2020) 596 [[arXiv:1903.02422](#)].
- [8] M. Chala, A. Lenz, A.V. Rusov and J. Scholtz, *ΔA_{CP} within the Standard Model and beyond*, *JHEP* **07** (2019) 161 [[arXiv:1903.10490](#)].
- [9] M. Saur and F.-S. Yu, *Charm CPV: observation and prospects*, *Sci. Bull.* **65** (2020) 1428 [[arXiv:2002.12088](#)].
- [10] HFLAV collaboration, *Averages of b-hadron, c-hadron, and τ -lepton properties as of 2021*, *Phys. Rev. D* **107** (2023) 052008 [[arXiv:2206.07501](#)].
- [11] M. Williams, *Observing CP Violation in Many-Body Decays*, *Phys. Rev. D* **84** (2011) 054015 [[arXiv:1105.5338](#)].
- [12] LHCb collaboration, *Observation of CP Violation in Charm Decays*, *Phys. Rev. Lett.* **122** (2019) 211803 [[arXiv:1903.08726](#)].
- [13] G. Valencia, *Angular Correlations in the Decay $B \rightarrow VV$ and CP Violation*, *Phys. Rev. D* **39** (1989) 3339.
- [14] A. Datta and D. London, *Triple-product correlations in $B \rightarrow V_1 V_2$ decays and new physics*, *Int. J. Mod. Phys. A* **19** (2004) 2505 [[arXiv:hep-ph/0303159](#)].
- [15] J.-P. Wang, Q. Qin and F.-S. Yu, *CP violation induced by T-odd correlations and its baryonic application*, [arXiv:2211.07332](#).
- [16] G. Durieux and Y. Grossman, *Probing CP violation systematically in differential distributions*, *Phys. Rev. D* **92** (2015) 076013 [[arXiv:1508.03054](#)].

- [17] G. Durieux, *CP violation in multibody decays of beauty baryons*, *JHEP* **10** (2016) 005 [[arXiv:1608.03288](#)].
- [18] Z.-H. Zhang, *Searching for CP violation through two-dimensional angular distributions in four-body decays of bottom and charmed baryons*, *Phys. Rev. D* **107** (2023) L011301 [[arXiv:2209.13196](#)].
- [19] M. Jacob and G.C. Wick, *On the General Theory of Collisions for Particles with Spin*, *Annals Phys.* **7** (1959) 404.
- [20] S.U. Chung, *A General formulation of covariant helicity coupling amplitudes*, *Phys. Rev. D* **57** (1998) 431.
- [21] A. Abashian et al., *The Belle detector*, *Nucl. Instr. and Meth. A* **479** (2002) 117.
- [22] S. Kurokawa and E. Kikutani, *Overview of the KEKB accelerators*, *Nucl. Instr. and Meth. A* **499** (2003) 1.
- [23] T. Abe et al., *Achievements of KEKB*, *Prog. Theor. Exp. Phys.* **2013** (2013) 03A001.
- [24] BELLE collaboration, *Physics Achievements from the Belle Experiment*, *Prog. Theor. Exp. Phys.* **2012** (2012) 04D001 [[arXiv:1212.5342](#)].
- [25] BELLE II collaboration, *Belle II technical design report*, [arXiv:1011.0352](#).
- [26] K. Akai, K. Furukawa and H. Koiso, *SuperKEKB collider*, *Nucl. Instrum. Meth. A* **907** (2018) 188 [[arXiv:1809.01958](#)].
- [27] BELLE-II DEPFET, PXD collaboration, *DEPFET pixel detector in the Belle II experiment*, *Nucl. Instrum. Meth. A* **936** (2019) 657.
- [28] BELLE-II DEPFET, PXD collaboration, *Commissioning and performance of the Belle II pixel detector*, *Nucl. Instrum. Meth. A* **987** (2021) 164875.
- [29] BELLE-II SVD GROUP collaboration, *The design, construction, operation and performance of the Belle II silicon vertex detector*, *JINST* **17** (2022) P11042 [[arXiv:2201.09824](#)].
- [30] D. Kotchetkov et al., *Front-end electronic readout system for the Belle II imaging Time-Of-Propagation detector*, *Nucl. Instrum. Meth. A* **941** (2019) 162342 [[arXiv:1804.10782](#)].
- [31] BELLE II collaboration, *Measurement of the integrated luminosity of data samples collected during 2019-2022 by the Belle II experiment*, [arXiv:2407.00965](#).
- [32] BELLE II FRAMEWORK SOFTWARE GROUP collaboration, *The Belle II Core Software*, *Comput. Softw. Big Sci.* **3** (2019) 1 [[arXiv:1809.04299](#)].
- [33] M. Gelb et al., *B2BII: Data Conversion from Belle to Belle II*, *Comput. Softw. Big Sci.* **2** (2018) 9 [[arXiv:1810.00019](#)].
- [34] D.J. Lange, *The EvtGen particle decay simulation package*, *Nucl. Instrum. Meth. A* **462** (2001) 152.
- [35] GEANT4 collaboration, *GEANT4—a simulation toolkit*, *Nucl. Instrum. Meth. A* **506** (2003) 250.
- [36] T. Sjostrand, S. Mrenna and P.Z. Skands, *PYTHIA 6.4 Physics and Manual*, *JHEP* **05** (2006) 026 [[arXiv:hep-ph/0603175](#)].
- [37] T. Sjöstrand, S. Ask, J.R. Christiansen, R. Corke, N. Desai, P. Ilten et al., *An Introduction to PYTHIA 8.2*, *Comput. Phys. Commun.* **191** (2015) 159 [[arXiv:1410.3012](#)].

- [38] S. Jadach, B.F.L. Ward and Z. Wąs, *The precision Monte Carlo event generator KK for two-fermion final states in e^+e^- collisions*, *Comput. Phys. Commun.* **130** (2000) 260 [[arXiv:hep-ph/9912214](#)].
- [39] E. Barberio, B. van Eijk and Z. Wąs, *PHOTOS: A universal Monte Carlo for QED radiative corrections in decays*, *Comput. Phys. Commun.* **66** (1991) 115.
- [40] PARTICLE DATA GROUP collaboration, *Review of particle physics*, *Phys. Rev. D* **110** (2024) 030001.
- [41] K. Hanagaki, H. Kakuno, H. Ikeda, T. Iijima and T. Tsukamoto, *Electron identification in Belle*, *Nucl. Instrum. Meth. A* **485** (2002) 490 [[arXiv:hep-ex/0108044](#)].
- [42] A. Abashian et al., *Muon identification in the Belle experiment at KEKB*, *Nucl. Instrum. Meth. A* **491** (2002) 69.
- [43] M. Milesi, J. Tan and P. Urquijo, *Lepton identification in Belle II using observables from the electromagnetic calorimeter and precision trackers*, *EPJ Web Conf.* **245** (2020) 06023.
- [44] M. Feindt and U. Kerzel, *The NeuroBayes neural network package*, *Nucl. Instrum. Meth. A* **559** (2006) 190.
- [45] BELLE collaboration, *Measurement of time-dependent CP asymmetries in $B^0 \rightarrow K_S^0 \eta \gamma$ decays*, *Phys. Rev. D* **97** (2018) 092003 [[arXiv:1803.07774](#)].
- [46] BELLE II ANALYSIS SOFTWARE GROUP collaboration, *Global decay chain vertex fitting at Belle II*, *Nucl. Instrum. Meth. A* **976** (2020) 164269 [[arXiv:1901.11198](#)].
- [47] BELLE collaboration, *Search for CP Violation in the Decay $D^+ \rightarrow K_S^0 K^+$* , *JHEP* **02** (2013) 098 [[arXiv:1212.6112](#)].
- [48] BELLE collaboration, *Evidence for CP Violation in the Decay $D^+ \rightarrow K_S^0 \pi^+$* , *Phys. Rev. Lett.* **109** (2012) 021601 [[arXiv:1203.6409](#)].